# Encoding and decoding of orbital angular momentum for wireless optical interconnects on chip

**Dengke Zhang, Xue Feng,* and Yidong Huang**

*State Key Lab. of Integrated Optoelectronics, Department of Electronic Engineering, Tsinghua University, Beijing 100084, China*

*x-feng@tsinghua.edu.cn

**Abstract:** Beams carried orbital angular momentum (OAM) are proposed for wireless optical interconnects on chip and a full scheme of encoding and decoding of OAM at single frequency is demonstrated with numerical simulation. With proposed structure, beams with OAM order of −3 to 4 are generated and four orders of them (0 to 3) are used to encode and decode data so that the increased data density of two folds is achieved. According to such results, we believe that if OAM is utilized as an additional dimension in wireless optical interconnects, the data density can be significantly increased since the adopted orders of OAM could be infinite in principle. Moreover, such improvement could be easily applied to the existing architecture without any more complex technology.



**OCIS codes:** (130.3120) Integrated optics devices; (130.4110) Modulators; (060.4510) Optical communications.

## References and links

1. L. Allen, M. W. Beijersbergen, R. J. Spreeuw, and J. P. Woerdman, "Orbital angular momentum of light and the transformation of Laguerre-Gaussian laser modes," Phys. Rev. A **45**(11), 8185–8189 (1992).
2. M. Padgett, J. Courtial, and L. Allen, "Light's orbital angular momentum," Phys. Today **57**(5), 35–40 (2004).
3. G. Molina-Terriza, J. P. Torres, and L. Torner, "Twisted photons," Nat. Phys. **3**(5), 305–310 (2007).
4. L. Allen and M. J. Padgett, "The Poynting vector in Laguerre-Gaussian beams and the interpretation of their angular momentum density," Opt. Commun. **184**(1-4), 67–71 (2000).
5. S. M. Barnett, "Optical angular-momentum flux," J. Opt. B Quantum Semiclassical Opt. **4**(2), S7–S16 (2002).
6. N. B. Simpson, L. Allen, and M. J. Padgett, "Optical tweezers and optical spanners with Laguerre-Gaussian modes," J. Mod. Opt. **43**(12), 2485–2491 (1996).
7. H. He, M. E. Friese, N. R. Heckenberg, and H. Rubinsztein-Dunlop, "Direct observation of transfer of angular momentum to absorptive particles from a laser beam with a phase singularity," Phys. Rev. Lett. **75**(5), 826–829 (1995).
8. K. T. Gahagan and G. A. Swartzlander, Jr., "Optical vortex trapping of particles," Opt. Lett. **21**(11), 827–829 (1996).
9. S. Fürhapter, A. Jesacher, S. Bernet, and M. Ritsch-Marte, "Spiral phase contrast imaging in microscopy," Opt. Express **13**(3), 689–694 (2005).
10. J. Lobera and J. Coupland, "Contrast enhancing techniques in digital holographic microscopy," Meas. Sci. Technol. **19**(2), 025501 (2008).
11. A. Mair, A. Vaziri, G. Weihs, and A. Zeilinger, "Entanglement of the orbital angular momentum states of photons," Nature **412**(6844), 313–316 (2001).
12. B. Thidé, H. Then, J. Sjöholm, K. Palmer, J. Bergman, T. D. Carozzi, Y. N. Istomin, N. H. Ibragimov, and R. Khamitova, "Utilization of photon orbital angular momentum in the low-frequency radio domain," Phys. Rev. Lett. **99**(8), 087701 (2007).
13. Z. Bouchal and R. Celechovský, "Mixed vortex states of light as information carriers," New J. Phys. **6**, 131 (2004).
14. J. Leach, M. J. Padgett, S. M. Barnett, S. Franke-Arnold, and J. Courtial, "Measuring the orbital angular momentum of a single photon," Phys. Rev. Lett. **88**(25), 257901 (2002).
15. G. Gibson, J. Courtial, M. Padgett, M. Vasnetsov, V. Pas'ko, S. Barnett, and S. Franke-Arnold, "Free-space information transfer using light beams carrying orbital angular momentum," Opt. Express **12**(22), 5448–5456 (2004).
16. R. Čelechovský and Z. Bouchal, "Optical implementation of the vortex information channel," New J. Phys. **9**(9), 328 (2007).
17. F. Tamburini, E. Mari, A. Sponselli, B. Thidé, A. Bianchini, and F. Romanato, "Encoding many channels on the

#174177 - $15.00 USD Received 10 Aug 2012; revised 19 Oct 2012; accepted 9 Nov 2012; published 15 Nov 2012

same frequency through radio vorticity: first experimental test," New J. Phys. **14**(3), 033001 (2012).
18. J. Wang, J.-Y. Yang, I. M. Fazal, N. Ahmed, Y. Yan, H. Huang, Y. Ren, Y. Yue, S. Dolinar, M. Tur, and A. E. Willner, "Terabit free-space data transmission employing orbital angular momentum multiplexing," Nat. Photonics **6**(7), 488–496 (2012).
19. R. G. Beausoleil, P. J. Kuekes, G. S. Snider, S. Y. Wang, and R. S. Williams, "Nanoelectronic and nanophotonic interconnect," Proc. IEEE **96**(2), 230–247 (2008).
20. S. Richard, "The Achievements and Challenges of Silicon Photonics," Adv. Opt. Technol. **2008**, 472305 (2008).
21. L. Tsybeskov, D. Lockwood, and M. Ichikawa, "Silicon photonics: CMOS going optical," Proc. IEEE **97**(7), 1161–1165 (2009).
22. M. Paniccia, "Integrating silicon photonics," Nat. Photonics **4**(8), 498–499 (2010).
23. A. Alù and N. Engheta, "Wireless at the Nanoscale: Optical Interconnects using Matched Nanoantennas," Phys. Rev. Lett. **104**(21), 213902 (2010).
24. S. M. Mohammadi, L. K. S. Daldorff, J. E. S. Bergman, R. L. Karlsson, B. Thidé, K. Forozesh, T. D. Carozzi, and B. Isham, "Orbital angular momentum in radio—a system study," IEEE Trans. Antenn. Propag. **58**(2), 565–572 (2010).
25. Y. F. Yu, Y. H. Fu, X. M. Zhang, A. Q. Liu, T. Bourouina, T. Mei, Z. X. Shen, and D. P. Tsai, "Pure angular momentum generator using a ring resonator," Opt. Express **18**(21), 21651–21662 (2010).
26. N. K. Fontaine, C. R. Doerr, and L. Buhl, "Efficient multiplexing and demultiplexing of free-space orbital angular momentum using photonic integrated circuits," in Optical Fiber Communication Conference, California, USA, March 4, 2012.
27. D. Dregely, R. Taubert, J. Dorfmüller, R. Vogelgesang, K. Kern, and H. Giessen, "3D optical Yagi-Uda nanoantenna array," Nat Commun **2**, 267 (2011).
28. N. K. Fontaine, C. R. Doerr, M. A. Mestre, R. Ryf, P. Winzer, L. Buhl, Y. Sun, X. Jiang, and R. Lingle, "Space-division multiplexing and all-optical MIMO demultiplexing using a photonic integrated circuit," in Optical Fiber Communication Conference, California, USA, March 4, 2012.
29. Q. Xu, B. Schmidt, S. Pradhan, and M. Lipson, "Micrometre-scale silicon electro-optic modulator," Nature **435**(7040), 325–327 (2005).
30. G. Reed, G. Mashanovich, F. Gardes, and D. Thomson, "Silicon optical modulators," Nat. Photonics **4**(8), 518–526 (2010).
31. H. Takahashi, S. Suzuki, K. Kato, and I. Nishi, "Arrayed-waveguide grating for wavelength division multi/demultiplexer with nanometre resolution," Electron. Lett. **26**(2), 87–88 (1990).

## 1. Introduction

Since the pioneering work of Allen et.al, the optical orbital angular momentum (OAM) has stimulated much interest [1–3]. Owing to unique characteristics of spiral flow of electromagnetic energy and helical wave-front [4,5], OAM could be applied on optical tweezers and spanner [6–8], light microscopy [9,10], quantum and wireless communications [11–13], etc. Specifically, the OAM is very attractive for data transmission due to the nature of unlimited number of potential states so that OAM beams can carry an infinite amount of data in principle [11,14]. It has been demonstrated that the wireless communications with OAM multiplexing can work in both optical and radio frequency domains with higher data rate and capacity [15–18].

As the development of CMOS technology, it becomes urgent to increase the transmission data rate in computer systems [19]. Among the proposed solutions, optical interconnect on chip is considered as the most promising one [20–22]. In 2010, A. Alu et al. proposed that wireless optical interconnects could be employed to obtain higher performances for communication on chip [23]. However, in the reported work of the wireless optical interconnects, only plane or spherical wave is considered. As mentioned above, if OAM could be employed for such systems, the transmission data rate could be dramatically increased and as a result, the power consumption per bit could be dramatically reduced.

In this work, aiming to exploit a new dimension for wireless optical interconnects, optical OAM is proposed for wireless optical links within layers or chips so that the data density can be increased. As the first step, encoding and decoding OAM on optical light with integrated structure on silicon chip are demonstrated with numerical simulation. The optical OAM is generated by a ring cavity with one input waveguide, in which the OAM order only depends on the mode order of ring. Therefore, optical OAM can be encoded by electro-optic tuning of the mode order of ring cavity at a certain wavelength with high speed. Moreover, the encoded OAM beam can be easily decoded using gratings and Mach-Zehnder interferometers. Based on such a coding approach with multi-nary symbol, the data density can be significantly increased by taking advantage of an additional dimension of OAM beams.

#174177 - $15.00 USD Received 10 Aug 2012; revised 19 Oct 2012; accepted 9 Nov 2012; published 15 Nov 2012

## 2. Generating beams with OAM on chip

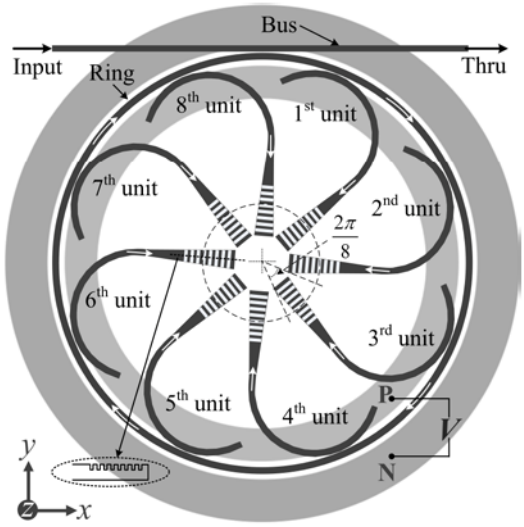


Fig. 1. The proposed structure with one ring, one bus waveguide and eight download units and each download unit is constituted by an arc waveguide and a grating. Two strips around the ring represent p-doped and n-doped regions for electrical tuning of the ring. The inset shows the profile of the output grating.

Figure 1 is the schematic of the proposed structure for producing and encoding optical OAM on chip. There are one ring cavity, one bus waveguide, and eight download units (each including an arc waveguide and a grating). The eight download units are equally coupled to the ring and equidistantly distributed around the circle, i.e. eight-fold rotationally symmetrical location. If the central frequency of input light, which is injected from the input-port of bus, deviates from the resonance of ring cavity, the light would pass through the thru-port of bus waveguide. On the contrary, if input light satisfies the resonance condition of ring cavity, it would be coupled into the ring and propagates along the ring as whispering-gallery-mode (WGM) and downloaded by each of the eight arc waveguides. Finally, the lights propagating in all arc waveguides would be combined and transformed into free space light (or travels in homogenous and isotropic medium) at the end of gratings. Since the phase shift of propagating light at each downloaded unit is successively varied, the phase of output light beam superposed from gratings would be azimuthally dependent. In other words, an OAM beam with azimuthal phase dependence of $\exp(il\varphi)$ could be generated, which is similar to the principle reported in Ref [24,25].

Specifically for the resonant light, the circumference of the ring ( $L$ ) and propagation constant of light ( $\beta$ ) satisfy the resonant relation:

$$\beta L = n\ 2\pi \tag{1}$$

where $n$ is the WGM order of light in the ring. The phase shift of a circle is $2n\pi$ along the ring so that the phase difference between each download unit is $(n \cdot 2\pi)/8$ and would be carried by light beam in free space. Here, considering the periodicity of phase shift in optical interference, the $n$ can be rewritten as

$$n = N\ p + m \tag{2}$$

where $N$ is the number of download units, $p$ is a positive integer, and $m$ is expressed as modulo $N$ with an integer value from 0 to $N-1$. Here, $N$ is considered as 8 and then $m$

#174177 - $15.00 USD Received 10 Aug 2012; revised 19 Oct 2012; accepted 9 Nov 2012; published 15 Nov 2012

can be taken as an integer from 0 to 7. Thus the effective phase difference ( $\Delta\phi_{eff}$ ) between any two adjacent download units is $(m \cdot 2\pi)/8$ and the total effective phase shift ( $\Delta\phi_{total}$ ) for a round circle is $2m\pi$. According to Eq. (2) and $\Delta\phi_{eff} = (m \cdot 2\pi)/8$, every eight adjacent WGM orders would be considered as a group with eight different $\Delta\phi_{eff}$ and the behaviors of each group are similar for generating OAM. According to Ref [26], $N$ arcs can produce $N$ types of OAM of beams with order taken from $-N/2$ to $N/2$. For case of $N = 8$, the relationship between OAM order $l$ and the parameter $m$ is

$$l = \begin{cases} m & (m \le 4) \\ m - 8 & (m > 4) \end{cases} \tag{3}$$

For further understanding of the produced OAM beam, three dimensional finite difference time domain (3D-FDTD) method is employed to calculate the near and far electromagnetic field distributions of the structure shown in Fig. 1. Such structure is assumed to be fabricated on silicon-on-insulator (SOI) substrate with top cladding silicon dioxide layer. The thickness and refractive indices of silicon/silicon dioxide layers are 340-nm/3-μm and 3.45/1.46, respectively. The radiuses of the ring and all arcs are 16 μm and 5 μm, respectively. To achieve the critical coupling state of ring cavity for obtaining maximum intensity of the WGM light, the distance between the bus and ring as well as those between arcs and ring should be carefully designed. Here, the optimized distances (edge to edge) are calculated as 20 nm and 60 nm, respectively. The width of all waveguides (ring, bus, and arcs) is 500 nm while that of grating is gradually increased to 2 μm within the length of 7 μm. All gratings are designed as the height of 100 nm, eight cycles with pitch of 500 nm and duty-cycle of 50%.

Figure 2(a) shows the calculated transmission spectrum at thru-port and each peak is corresponding to a certain WGM order of light in the ring. Here, a group of eight resonant peaks in the telecom band (192~198 THz or 1.52~1.56 μm) are chosen. The corresponding orders of WGM ( $n$ and $m$ ) and the OAM ( $l$ of −3~4) are depicted in Fig. 2(a). The calculated near and far field distributions for $l = 0, 1,$ and $-1$ are shown in Figs. 2(b-d) as representative examples.

For $m = 0$ the near field distribution is a series of concentric circles (Fig. 2(b1)) while the phase difference is nearly zero along each circle in the far field phase distribution (Fig. 2(b2)) so that it corresponds to $l = 0$. For $m = 1$ and $m = 7$ (Figs. 2(c1) and (d1)), the near field distributions are very similar to each other. However, the corresponding far fields are quite different (Figs. 2(c2) and (d2)), where $|\Delta\phi_{total}| = 2\pi$ and the phase rotation directions are opposite, which indicates that beams of $l = 1$ and $l = -1$ are generated. For more clarity, the instantaneous electric field distributions are displayed in Media 1, Media 2, Media 3 for $l = 0, 1,$ and $-1$. And for beams with higher order OAM, the near average-steady and instantaneous electric field distributions are displayed in Fig. 2(e) and Media 4, Media 5, Media 6, Media 7, and Media 8, respectively. These results indicate that beams with OAM can be generated with proposed integrated structure and the order of OAM is determined by the WGM order following the relationship of Eq. (3).

#174177 - $15.00 USD Received 10 Aug 2012; revised 19 Oct 2012; accepted 9 Nov 2012; published 15 Nov 2012

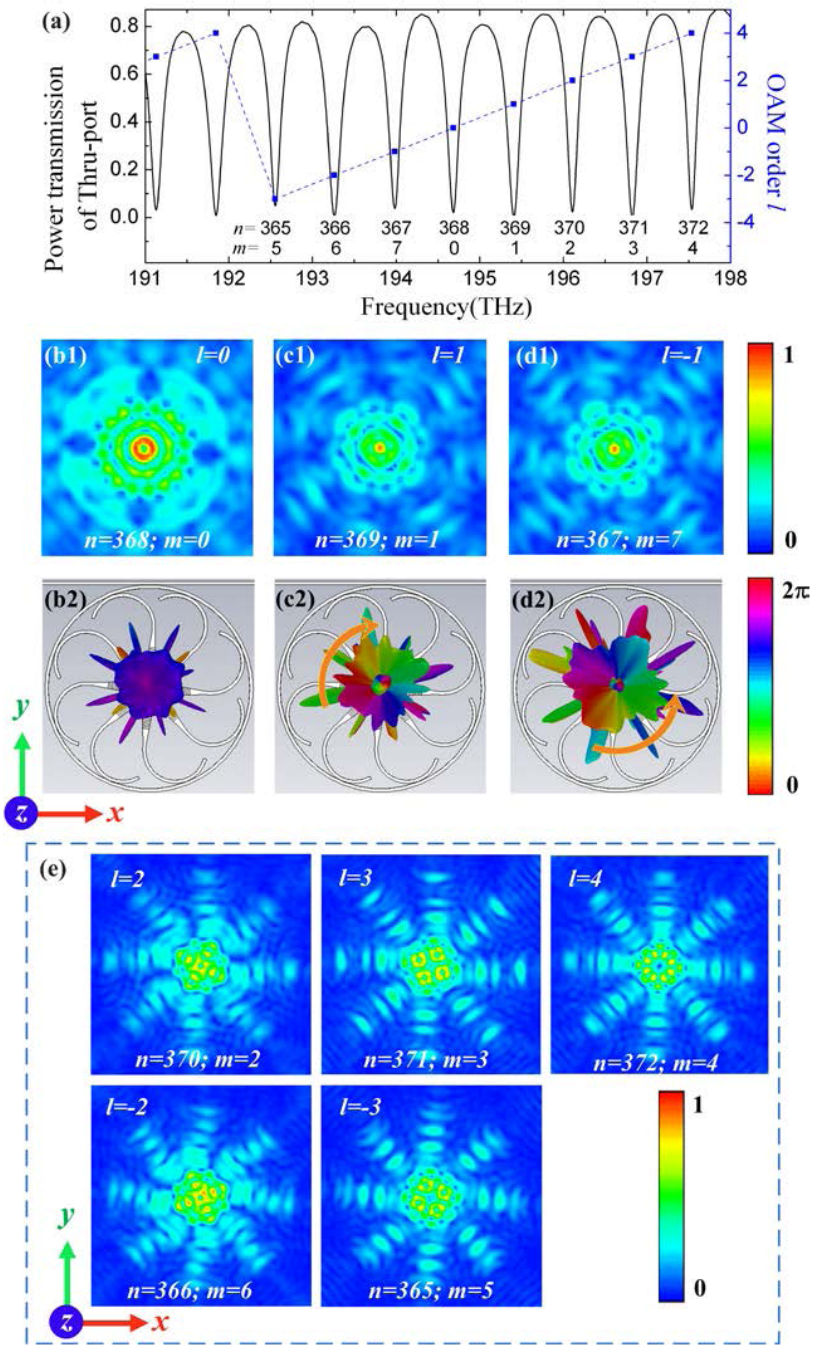


Fig. 2. (a) Optical power transmission at thru port of the structure and each resonant peak corresponds to a beam with OAM. Every eight resonant frequencies are grouped to generate eight different kinds of OAM of order $l$ from −3 to 4. (b1-d1) Near field patterns of electrical component of OAM beams with order of 0, 1 and −1 (Media 1, Media 2, and Media 3). (b2-d2) Corresponding far field phase patterns of azimuthal electrical components. For $l$ = 0, phase difference is zero along a circle, while for $l$ = 1 and −1, both the phase shifts are $2\pi$ along a circle but with opposite rotation direction. (e) Near field patterns of beams with OAM order of 2 to 4, −2, and −3 (Media 4, Media 5, Media 6, Media 7, and Media 8).

#174177 - $15.00 USD Received 10 Aug 2012; revised 19 Oct 2012; accepted 9 Nov 2012; published 15 Nov 2012

### 3. Encoding and decoding data with OAM beam on the single frequency carrier

In order to convey information with OAM states, it is required to modulate different orders of OAM on optical carrier at a certain wavelength. With the proposed structure, different OAM orders could be encoded by varying the WGM order of ring cavity following Eq. (3). Furthermore, the decoding can be done by receiving elements such as optical gratings or nano-antennas, which relies on detecting phase information of beams with OAM at different azimuthal distributions as Ref [26–28]. In principle, $N$ types of OAM of beams can be produced by $N$ arcs and could be distinguished by $N$ receiving elements. However, due to the beam spreading of different order of OAM, only half or less of the total number of types can be clearly and easily distinguished [26]. So only quaternary encoding and decoding ($l = 0$, 1, 2, and 3) are considered although there are eight download units. As shown in Fig. 3, OAM is encoded on light beam at layer1 and decoded by superposition of lights from four receiving elements at layer2 which are rotationally symmetric on a circle.

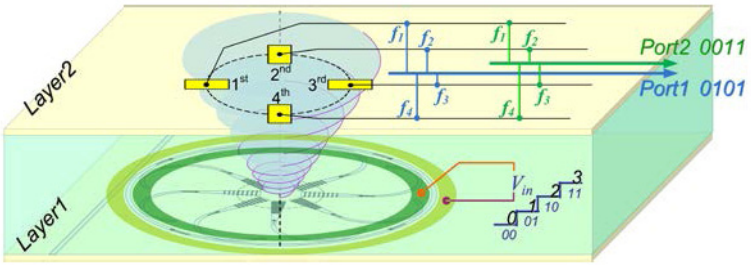


Fig. 3. In layer1, the input binary signals are transformed to quantized quaternary voltage signals and then applied on p-n junctions, and consequently four different types of OAM beams are generated. In layer2, the encoded beam is received by four elements and the signals are recovered by weighted superposition (weighting factors are represented by $[f_1, f_2, f_3, f_4]$) among received lights and exported to two ports in binary format.

According to Eq. (1), the WGM order at a certain frequency could be adjusted by changing $\beta$, which could be easily achieved by varying the refractive index of Si ($n_{Si}$). As demonstrated for silicon optical intensity modulator, the $n_{Si}$ could be varied by carrier injection or depletion with p-n junctions with very high speed [29,30]. As shown in Fig. 1, we assume that there is a proper p-n junction around the ring cavity for varying $n_{Si}$, which are similar to the structure of silicon ring modulator [29]. Then via properly adjusting the refractive index, the WGM order at a certain optical frequency could be tuned. As an example, the WGM order at frequency of 194.68 THz is 368 ($m = 0$) while it could be tuned to 369 ($m = 1$) or 367 ($m = 7$) with index variation ($\Delta n_{Si}$) of 0.0116 or −0.0116 and the OAM order is tuned from $l = 0$ to 1 or −1. The optical transmission spectra at the thru port of bus waveguide with varied $\Delta n_{Si}$ are shown in Fig. 4(a) and the corresponding near field patterns are shown in Figs. 4(b-d). Similarly, higher order of OAM also can be obtained by increasing $\Delta n_{Si}$. Furthermore, Fig. 4(e) shows the calculated relationship between OAM order $l$ and $\Delta n_{Si}$. Because $\Delta n_{Si}$ is determined by the applied voltage on p-n junction, the quantized voltage signal can be encoded to different order of OAM with our proposed structure. Specifically for structure shown as layer1 in Fig. 3, the input binary signals are transformed to quantized quaternary voltage signals in electric domain and applied on p-n junctions so that four different orders of OAM beams are consequently generated. Comparing to encoding data using OAM at different wavelengths, such approach is more efficient in bandwidth utilization and can increase the data rate due to multi-nary coding assisted by the additional dimension of OAM.

#174177 - $15.00 USD Received 10 Aug 2012; revised 19 Oct 2012; accepted 9 Nov 2012; published 15 Nov 2012

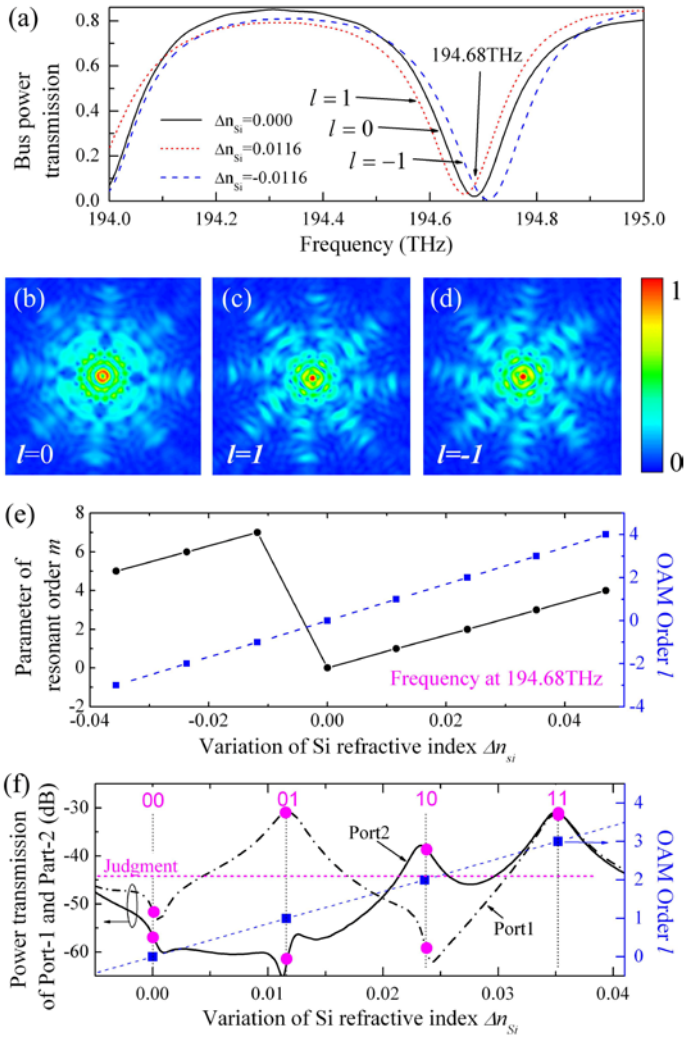


Fig. 4. (a) The OAM order is tuned at the same frequency of 194.68 THz following tuning WGM order which is achieved by tuning of silicon refractive index. The OAM order is tuned to 1 or −1 from 0 with $\Delta n_{Si}$ = 0.0116 or −0.0116 (b-d) Near field patterns for beams at frequency of 194.68 THz of $l = 0, 1$ ,and −1 corresponding to peaks shown in (a) . (e) Relationships of $m$ and $l$ versus the variation of silicon refractive index ( $\Delta n_{Si}$ ). (f) Relationships of power transmission of ports (Port-1 and Port-2) and order of OAM versus variation of refractive index. At OAM order $l = [0, 1, 2, 3]$, the corresponding recovered binary signals of $[00, 01, 10, 11]$ are recovered and exported through Port-1 and Port-2.

Decoding signals from beams with OAM are achieved by two steps: free-space light is received and transformed to multi-guided lights using gratings, and then signals are recovered by superposition of the multi-guided lights. Here, we assume that the input binary signals of $[00, 01, 10, 11]$ correspond to $\Delta n_{Si}$ of $(0.0116 \times [0, 1, 2, 3])$ and OAM beams of $l = [0, 1, 2, 3]$ are generated at frequency of 194.68 THz in succession in layer1. Then the encoded OAM beams propagate to layer2 with distance of 3 μm and are received by the four

#174177 - $15.00 USD Received 10 Aug 2012; revised 19 Oct 2012; accepted 9 Nov 2012; published 15 Nov 2012

gratings with the same structure parameters as the gratings in the layer 1. Thus, the encoded free-space light with OAM is received and transferred to four-guided lights by four gratings. Although the phase shift of received light of each grating is time-varied, there is still a stable phase difference of $2\pi l / 4$ between any two adjacent gratings so that the binary signals could be recovered by coherent superposition among the four-guided lights, which could be achieved by Mach-Zehnder interferometers (MZIs) or arrayed-waveguide gratings [31]. Since each OAM state represents a quaternary number (i.e. two binary numbers), the recovered signals will be exported to two binary outputs at each OAM state using these four-guided lights. The procedure of recovering signals is introduced with more details in Appendix-A. Here, with weighting factor depicted by Eq. (5) in Appendix-A, the relationships between outputs of two ports and OAM order versus $\Delta n_{Si}$ is shown in Fig. 4(f). It could be seen that OAM order of 0~3 are encoded by varying $n_{Si}$ and the signals are successfully recovered and exported to binary optical signals at port1 and port2. It should be mentioned that the free carrier absorption of electrical tuning is not considered in our simulation. The required variation of $\Delta n_{Si}$ is as large as 0.035 so that free carrier absorption introduced by electrical injection should be taken into account. For a practical device, one possible solution is to adopt a ring with much larger radius so that the requirement of $\Delta n_{Si}$ could be small enough.

With such quaternary coding, the transmitted data rate on chip could be increased two folds (deduced from $\log_2 4$ for quaternary signal) and the power consumption per bit could be reduced by half in succession. Obviously, if higher multi-ary coding is employed, data rate could be dramatically increased as $\log_2 N$ folds for $N$ -nary signal, and more details can be found in Appendix-B. Here, only a simple case of quaternary coding is considered in order to demonstrate the operating principle more clearly. Actually, there is no physical limit to achieve higher order OAM coding with our proposed structure. Furthermore, it should be mentioned that the proposed structure could be easily applied on the existing optical interconnects architecture and what should be done is replacing the intensity modulator with the encoder and adding a decoder before the photodetectors.

It is worth pointing out that such proposed structure is not only potential for wireless optical interconnects, moreover, but also can serve as OAM generator or OAM modulator for free-space optical communications, quantum communications, and optical manipulations. Among most of these applications, if the tuning speed is not very critical, thermal tuning can also be adopted to switch from several to dozens of OAM states since silicon refractive index could be varied within a rather wide range with thermo-optic effect.

## 4. Summary

A full solution of adopting optical OAM for wireless optical interconnects on chip is proposed, which includes generation of OAM beams and encoding/decoding data on OAM. With the help of numerical simulation, we found that taking full advantage of the OAM correctly can increase the data density substantially in the wireless optical interconnections on chip. Furthermore, the fabrication of the proposed structure is compatible with CMOS technology and the existing optical interconnects architecture. And we believe that the integrated OAM generator or modulator also can be applied for free-space optical communications, quantum communications, and optical manipulations with distinguished feature.

#174177 - $15.00 USD Received 10 Aug 2012; revised 19 Oct 2012; accepted 9 Nov 2012; published 15 Nov 2012

## Appendix

*A*

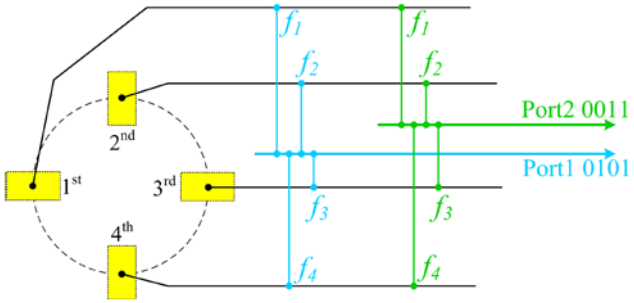


Fig. 5. A schematic of structure for receiving and recovering signal. Four yellow rectangles represent the receiving elements, such as gratings or optical nano-antennas. Then the received lights are combined with weighting factors of $[f_1, f_2, f_3, f_4]$ to recover the signals in binary form.

In the following calculation, we consider the case: four orders of OAM are produced ($l = 0$, 1, 2, and 3) with transformed quaternary voltage signals while four gratings or optical antennas are adopted to distinguish them. As shown in Fig. 5, if the initial phase of light received by first antenna is set as 0, the received field ($E_r^1$) can be expressed as $A_r e^{-j0}$. Then the received field ($E_r^q$) from $q$ th antenna could be consequently expressed as $E_r^q = A_r e^{-jq\cdot(2\pi l)/4}$. Obviously, the phase shift is related to the OAM order. With the help of such distinct phase shift of the four received lights, the signals can be recovered by weighted combination with optical interference so that decoding of OAM order could be achieved. In our simulation case, the OAM order of $l$ is encoded with 2-bit binary form and two output ports are required for output signals in binary form. The weighting factor between four-guided light and two output ports could be defined as a 2 × 4 matrix of $[f_{mn}]$. The required weighting factor could be deduced by the followed relation:

$$
\begin{array}{c}
\qquad\qquad\qquad\qquad \textit{Received lights} \qquad\qquad\qquad\qquad\qquad \textit{Output ports} \\
\qquad\quad 1st \qquad\qquad 2nd \qquad\qquad 3rd \qquad\qquad 4th \qquad\qquad \textit{port}\,2 \;\; \textit{port}\,1 \\
\begin{array}{l} l=0 \rightarrow \\ l=1 \rightarrow \\ l=2 \rightarrow \\ l=3 \rightarrow \end{array}
\begin{bmatrix}
A_r e^{-j0\cdot(2\pi\cdot 0/4)} & A_r e^{-j1\cdot(2\pi\cdot 0/4)} & A_r e^{-j2\cdot(2\pi\cdot 0/4)} & A_r e^{-j3\cdot(2\pi\cdot 0/4)} \\
A_r e^{-j0\cdot(2\pi\cdot 1/4)} & A_r e^{-j1\cdot(2\pi\cdot 1/4)} & A_r e^{-j2\cdot(2\pi\cdot 1/4)} & A_r e^{-j3(2\pi\cdot 1/4)} \\
A_r e^{-j0\cdot(2\pi\cdot 2/4)} & A_r e^{-j1\cdot(2\pi\cdot 2/4)} & A_r e^{-j2\cdot(2\pi\cdot 2/4)} & A_r e^{-j3\cdot(2\pi\cdot 2/4)} \\
A_r e^{-j0\cdot(2\pi\cdot 3/4)} & A_r e^{-j1\cdot(2\pi\cdot 3/4)} & A_r e^{-j2\cdot(2\pi\cdot 3/4)} & A_r e^{-j3\cdot(2\pi\cdot 3/4)}
\end{bmatrix}
\begin{bmatrix} f_1 \\ f_2 \\ f_3 \\ f_4 \end{bmatrix}
=
\begin{bmatrix} 0 & 0 \\ 0 & 1 \\ 1 & 0 \\ 1 & 1 \end{bmatrix}
\end{array}
\tag{4}
$$

Then, for decoding four orders of OAM, the matrix of weighting factors is

$$
\begin{bmatrix} f_1 \\ f_2 \\ f_3 \\ f_4 \end{bmatrix}
=
\begin{bmatrix}
0.50+0.00i & 0.50+0.00i \\
-0.25+0.25i & 0.00+0.00i \\
0.00+0.00i & 0.50+0.00i \\
-0.25-0.25i & 0.00+0.00i
\end{bmatrix}
=
\begin{bmatrix}
(1/2)e^{i0} & (1/2)e^{i0} \\
\left(\sqrt{2}/4\right)e^{i(3\pi/4)} & 0 \\
0 & (1/2)e^{i0} \\
\left(\sqrt{2}/4\right)e^{i(5\pi/4)} & 0
\end{bmatrix}
\tag{5}
$$

From Eq. (5), the weighting factor is complex, which could be obtained by controlling optical intensity and phase behind the gratings. For intensity control, it could be easily achieved by using directional couplers while the optical phase could be varied by inserting a

#174177 - $15.00 USD Received 10 Aug 2012; revised 19 Oct 2012; accepted 9 Nov 2012; published 15 Nov 2012

phase shifter before the superposition using Mach-Zehnder interferometers or arrayed-waveguide gratings. Such process for decoding and derivation of weighting factors can be easily extended to more orders of OAM of beams.

*B*

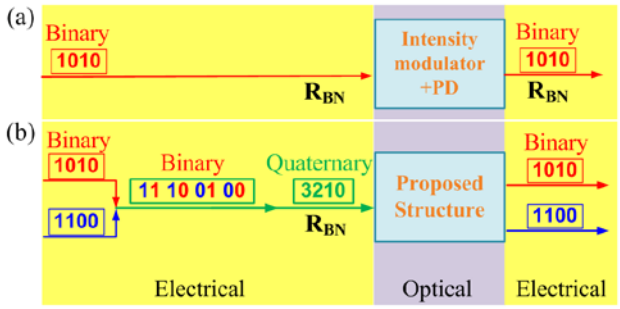


Fig. 6. Schematic of transmission procedures for (a) normal system (including intensity modulator and photodetector) and (b) proposed system

The data processing procedures for normal binary transmission system and our proposed system are depicted in Fig. 6(a) and 6(b), respectively. For such two systems, the symbol rate ($R_{BN}$) are supposed to be the same since $R_{BN}$ is only determined by speed of modulation. For a normal system, there are an intensity modulator (such as integrated microring or Mach-Zehnder modulator) and a photodetector. The input binary signals are directly encoded, thus the bit rate ($R_b$) is equal to the symbol rate ($R_{BN}$). For our proposed one, the input binary signals are firstly transformed to quaternary signals in electric domain and then are encoded. Thus, $R_b$ is equal to $(\log_2 4)*R_{BN}$ due to modulation of quaternary signals, namely the transmission date rate is increased two folds. Similarly, for coding with $N$ -nary signals, data rate could be increased $\log_2 N$ folds.

**Acknowledgments**

The authors would like to thank Dr. W. Zhang, Dr. F. Liu, Dr. K.Y. Cui, Dr. Q. Zhou, and H. Yan for their valuable discussions and helpful comments. This work was supported by the National Basic Research Program of China (No. 2011CBA00608, 2011CBA00303, 2011CB301803, and 2010CB327405), and the National Natural Science Foundation of China (Grant Nos. 61036011 and 61036010).

#174177 - $15.00 USD Received 10 Aug 2012; revised 19 Oct 2012; accepted 9 Nov 2012; published 15 Nov 2012